Mesh Objective Stochastic Simulations of Quasibrittle Fracture

Anna Gorgogianni[1], Jan Eliáš[2], and Jia-Liang Le[3]

Abstract: Continuum finite element (FE) modeling of damage and failure of quasibrittle structures suffers from the spurious mesh sensitivity due to strain localization. This issue has been addressed for deterministic analysis through the development of localization limiters. This study proposes a mechanism-based model to mitigate the mesh sensitivity in stochastic FE simulations of quasibrittle fracture. The interest is placed on the analysis of large-size structures, where the mesh size is conveniently chosen to be larger than the width of the fracture process zone as well as the correlation length of the random fields of constitutive properties. The present model is formulated within the framework of continuum damage mechanics. Two localization parameters are introduced to describe the evolution of the damage pattern of each finite element. These parameters are used to guide the energy regularization of the constitutive law, as well as to formulate the mesh-dependent probability distributions of constitutive properties. Depending on the prevailing damage pattern, different energy regularization schemes and mesh dependence of the probability distribution functions are used in the constitutive law. The model is applied to simulate the stochastic failure behavior of quasibrittle structures of different geometries featuring different failure processes including damage initiation, localization, and propagation. It is shown that using fixed probability distribution functions of constitutive properties could lead to strong mesh dependence of the prediction of the mean and variance of the peak load. The probability distribution functions of constitutive properties must be linked to the damage pattern, which may evolve during the failure process. Such a mechanism-based modeling of the probability distributions of constitutive properties is essential for mitigating the spurious mesh sensitivity in stochastic FE analysis of quasibrittle fracture.

1. Introduction

The importance of probabilistic analysis of structural behavior has become increasingly evident due to the fact that no engineering structures can be made risk free. Recent focuses have been placed on structures made of quasibrittle materials, which are heterogeneous materials with brittle constituents. Typical examples include tough ceramics, composites, concrete, rock, etc. The salient feature of quasibrittle materials is that, except for few loading scenarios (e.g. under high confining stresses), they generally exhibit a strain-softening behavior. This gives rise to localization instability [32, 3, 31, 16], which has profound implications for reliability analysis of quasibrittle structures. To capture the mechanism of damage localization in a probabilistic setting, a finite weakest-link model was developed for the strength distribution of quasibrittle structures failing at macrocrack initiation [8, 5, 20, 4]. The key result of the model is that it predicts a strong size effect on the probability distribution of structural strength, which transitions from a Gaussian distribution with a grafted far-left power law tail to a two-parameter Weibull distribution as the structure size increases. The finite weakest-link model provides an analytical expression of the strength distribution of quasibrittle structures, which is further used to derive the size-dependent safety factors for structural design [19, 4]. A more general probabilistic model, called the fishnet model, was recently developed for quasibrittle structures [24, 25]. The model can capture both localized and distributed damage mechanisms. However, the weakest-link model and fishnet model are mostly applied to structures of simple geometries, such as tension and flexural specimens. For more complex structural geometries under multiaxial stress states, it is inevitable to resort to stochastic simulations, which involve nonlinear constitutive models with random material properties [36, 35, 1].

[1]Department of Civil, Environmental, and Geo- Engineering, University of Minnesota.
[2]Institute of Structural Mechanics, Faculty of Civil Engineering, Brno University of Technology.
[3]Department of Civil, Environmental, and Geo- Engineering, University of Minnesota, Minneapolis, Minnesota. Corresponding author.

It is well acknowledged that localization instability leads to the spurious mesh sensitivity in finite element (FE) simulations [2, 7, 3]. Over the past four decades, various numerical approaches, generally referred to as the localization limiters, have been developed to mitigate the mesh dependence in FE simulations. The early attempt includes the crack band model [7], in which the post-peak behavior of the stress-strain curve is adjusted so as to preserve the fracture energy. The model assumes the scenario of fully localized damage. The main advantage of the crack band model is that it can be applied to large mesh sizes and is easy to implement in FE codes. Recently, a more general energy regularization method was proposed [13]. In the model, the tangential stiffness of the finite element is adjusted based on the prevailing damage pattern, which evolves during the loading process. It was shown that the model is capable of preserving the correct energy dissipation for various damage patterns including both diffused and localized damages, which is more versatile than the crack band model.

The other class of the localization limiters includes the nonlocal integral and gradient models [30, 29, 10]. In these models, the state variables responsible for the inelastic behavior of a local material point are made dependent not only on the local material response but also on the response of its neighborhood. The key feature of the nonlocal models is that they involve a length scale that defines the size of the nonlocal influence zone. To capture the nonlocality, nonlocal models require fine mesh sizes, which makes them inefficient for simulations of large-size structures. In addition, the treatment of nonlocality for material points that are close to the structural boundary still remains an unresolved issue [18, 6, 4].

All the existing localization limiters were developed for deterministic analysis, and few studies have investigated the mesh dependence in stochastic FE simulations [22]. However, some recent studies have revealed the challenge in stochastic simulations of quasibrittle fracture. Following the crack band model, we consider each finite element to represent a material element of finite size. Its constitutive properties no longer represent the behavior of a material point, but the behavior of a material element. The finite weakest-link model suggests that, if damage localization occurs, the strength distribution of material elements must depend on the element size [8, 20, 4]. This size dependence has been demonstrated by numerical simulations [11, 21]. Meanwhile, these studies have further shown that the size dependence of strength distribution is strongly influenced by the prevailing damage mechanism. These results indicate that, for stochastic FE simulations, the probability distribution functions of the constitutive properties should be formulated based on the damage mechanism, and a direct consequence is that the distribution functions could depend on the size of the FE mesh.

Some early studies adopted the Weibull distribution to determine the dependence of constitutive properties on the mesh size [23, 27]. The Weibull distribution implies a damage localization mechanism, in which the size of localized damage zone is negligibly small compared to the mesh size [4]. Clearly these conditions are not fulfilled in FE models, and therefore the Weibull distribution is inapplicable for probability distribution of constitutive properties of finite element mesh. In a recent study [22], it was proposed to use a finite weakest-link model for the strength properties of finite elements. The model also takes into account the effect of propagating damage on the strength distribution. However, it neglects the formulation of strength distribution for the case of diffused damage.

This paper presents a general computational framework for stochastic simulations of quasibrittle damage and fracture. The focus is placed on the scenario where the finite element mesh size is larger than the autocorrelation length of the underlying random field of material properties, typically several times the size of material inhomogeneities [14]. This is often a desirable choice for numerical simulations of large-size structures. The probability distribution functions of constitutive properties are derived based on the prevailing damage mechanism, which at the same time also governs the energy regularization of the overall constitutive behavior. The paper is planned as follows: Sec. 2 presents a simple demonstration of the issue of mesh dependence in stochastic FE analysis; Sec. 3 presents the stochastic constitutive model; Sec. 4 discusses the formulation of the probability distributions of constitutive properties; and Sec. 5 presents the numerical studies of ceramic specimens of different geometries.

2. Demonstration of Mesh Dependence in Stochastic Analysis

We first present a simple demonstration of the spurious mesh dependence in stochastic FE simulations of quasibrittle fracture. Consider a uniaxial tension specimen of length $L = 1$ m and cross-sectional area $A = 5 \times 10^{-4}$ m^2 (Fig. 1a). It is made of a quasibrittle material, which exhibits a simple linear strain-softening constitutive behavior (Fig. 1b). The specimen is now sub-divided into several elements along its length. It has been well known that, according to the second law of thermodynamics, the strain-softening behavior will cause damage localization into one element [2, 3]. In other words, only one element will experience strain softening, and the rest will undergo unloading. Consequently, the calculated total energy dissipation of the specimen would depend on the number of elements, which is physically inadmissible. In a deterministic setting, the mesh dependence of the global structural response can be mitigated by adjusting the post-peak tangential stiffness based on the element size so that the fracture energy is preserved, (i.e. $\gamma l_e = G_f$ where γ = area under the stress-strain curve, l_e = element length, and G_f = fracture energy), as done in the crack band model [7, 9]. The constitutive parameters are Young's modulus, tensile strength, and fracture energy.

Now consider the same problem in a stochastic setting, where each element has random tensile strength f_t and fracture energy G_f. We consider that both f_t and G_f follow Gaussian distributions, as a demonstration. It is assumed that these two properties are mutually independent, and each property is statistically independent across different elements. In this analysis, we take $E = 20$ GPa, mean tensile strength = 2.4 MPa, mean fracture energy = 90 J/m^2, and the coefficients of variation of f_t and G_f = 7.5%. To calculate the load-displacement response, we impose the equilibrium condition, that is the stress σ_i in any element is equal to P/A, and calculate the end displacement by $\Delta = \sum_{i=1}^{n} \epsilon_i l_e$, where P = applied load, $n = L/l_e$, and ϵ_i = strain in element i. The stress-strain curve of a single element is adjusted according to the element size using the crack band model.

To investigate the effect of discretization on the predicted stochastic response, we consider three element sizes, $l_e = 50,\ 100,\ 200$ mm. For each case, a total of 200 realizations are used to calculate the stochastic response of the load-displacement curve. Figs. 2a and b show the cumulative distribution functions (cdfs) of the peak load P_m and the total energy dissipation Γ (i.e. area under the load-deflection curve). It is seen that the predicted cdf of P_m depends strongly on the element size whereas the cdf of Γ does not.

This behavior can be explained by the fact that P_m is governed by the minimum strength of all the elements. Since the tensile strengths of the elements are statistically independent, the cdf of P_m can be calculated by the weakest-link model:

$$\text{Prob}(P_m \leq P) = 1 - [1 - P_1(P/A)]^n \tag{1}$$

where $P_1(x)$ = strength cdf of a single element. Based on Eq. 1, it is evident that the cdf of P_m would depend on n, or equivalently on the element size l_e. In contrast, the total energy dissipation of the bar is equal to the energy expended to completely damage a single element. Since the crack band model is able to regularize the energy dissipation for localized damage, the computed cdf of Γ is insensitive to the mesh size.

This simple example shows that energy regularization alone is insufficient for mitigating the mesh dependence in stochastic analysis. Eq. 1 indicates that, to ensure a mesh-independent cdf of P_m, we must consider $P_1(x)$ to vary with the element size. This size dependence is closely tied with the failure mechanism. Consider the element size is larger than the width l_0 of the damage localization zone, which represents a material characteristic length. If we further assume that the strengths of material elements of size l_0 are statistically independent, then $P_1(x)$ can be written by $P_1(x) = 1-[1 - P_0(x)]^{n_e}$, where $n_e = l_e/l_0$ and $P_0(x)$ = strength cdf of a material element of size l_0. Evidently, $P_1(x)$ is strongly dependent on the element size l_e. Substitution of the expression of $P_1(x)$ into Eq. 1 yields a mesh-independent prediction of the cdf of P_m.

The foregoing analysis shows that the issue of mesh dependence in stochastic analysis is closely related to the formulation of probability distribution functions of constitutive properties. The essential point is that the constitutive properties represent the behavior of a material element of finite size. Consequently, the cdf of constitutive properties could exhibit strong dependence on the element size, which must be taken into account in the stochastic analysis. In the aforementioned example, the specimen suffers damage localization right away when a single element reaches its peak strength, and the location of damage zone is random. Such a simple failure mechanism can be handled adequately by the weakest-link statistics, which naturally yields a size-dependent strength cdf of material element. However, in many cases, the failure mechanism of the structure is much more complicated. For instance, it may involve transitioning from diffused damage to localized damage. Therefore, a general probabilistic model of the constitutive properties is required.

3. Description of Constitutive Model

In this study, we consider an isotropic continuum damage model, which can be written in a general form as

$$\boldsymbol{\sigma} = f(\omega)\boldsymbol{C} : \boldsymbol{\epsilon} \tag{2}$$

where $\boldsymbol{C}$ is the elastic stiffness tensor, ω is a scalar damage variable ranging from 0 (intact state) to 1 (fully damaged state), $\boldsymbol{\epsilon}$ is the infinitesimal strain tensor, and $f(\omega)$ is a function which describes stiffness degradation of the bulk material due to damage. The degradation function $f(\omega)$ is monotonically non-increasing (i.e. $\mathrm{d}f/\mathrm{d}\omega \leq 0$), and has the maximum value of one at $\omega = 0$ and the minimum value of zero at $\omega = 1$.

It should be pointed out that the present model is suitable for describing a single damage mode, such as tensile failure. For more complicated mixed-mode failures, one could introduce a damage tensor. Since the objective of this study is not on constitutive modeling but on the treatment of the probability distribution functions of constitutive properties, we will present our formulation within the context of an isotropic damage model.

Following the previous study [13], we formulate the damage evolution law by treating each finite element as a material element of finite size. Here we limit our attention to finite elements with linear shape functions. To define the geometrical dimensions of the finite element for the purpose of constitutive modeling, we calculate the average strain tensor of the finite element, and denote the direction of the maximum principal strain by a unit vector $\vec{n}_g$. We define the element size h_1 as the length of the element along the direction of vector $\vec{n}_e$ passing through the centroid of the element, where $\vec{n}_e = \vec{n}_g$ before damage occurs, whereas after damage initiation $\vec{n}_e$ is fixed to be vector $\vec{n}_g$ measured at the onset of damage. Hereafter we refer to $\vec{n}_e$ as the principal vector of the element. With the definition of h_1, we can define h_2 as the size of the element in the orthogonal direction such that $h_1 h_2$ is equal to the area of the finite element (Fig. 3a).

It should be noted that, if one uses high-order elements, strain localization could occur in one integration point, and the remaining integration points would experience unloading [17]. In this case, we need to determine the effective size of material element, h_1, that corresponds to a single Gauss point. Recent studies have investigated this length parameter for the formulation of localization limiters for high-order elements [17].

For a given finite element, we consider that the crack will form in the direction perpendicular to the principal vector $\vec{n}_e$. Note that this direction is fixed upon damage initiation, which corresponds to the fixed crack model [9]. A common interpretation of the damage parameter is to consider that ωh_2 represents the crack length a. For tension-dominant damage, the energy expended for propagation of a single crack by distance δa can then be written as $G_f h_2 \delta\omega$ (G_f = mode I fracture energy). For quasibrittle materials, a finite-size fracture process zone (FPZ) forms at the crack tip. The FPZ length is related to the Irwin characteristic length, and its width h_0 represents a critical material length scale in the present model.

We postulate that the damage evolution is governed by a free energy function Y such that the energy release (per unit thickness) from the entire element due to an increment $\delta\omega$ can be written as $h_1 h_2 \delta Y$. By considering several cracks propagating simultaneously (Fig. 3b), we can write the following energy balance equation:

$$\frac{\partial Y}{\partial \omega} + \frac{n_b \bar{G}_f}{h_1} = 0 \tag{3}$$

$$\bar{G}_f = \frac{\sum_{i=1}^{k_b-1} G_{fi} + (n_b + 1 - k_b)\, G_{fk_b}}{n_b} \tag{4}$$

where n_b = number of active FPZs in the damage zone of width h_d, $\bar{G}_f$ = average of the fracture energies of n_b number of FPZs, G_{fi} = fracture energy associated with ith FPZ, and k_b = the least integer that is greater than or equal to n_b. In Eq. 3, we treat G_{fi} to be a random variable since the fracture energy exhibits a spatial randomness due to material heterogeneity. Note that in Eq. 4 we consider that there are $k_b - 1$ FPZs developed with full width, and the last FPZ may not have its full width because n_b may not be an integer. Eq. 3 represents a general energy regularization scheme, which recovers the purely localized damage ($n_b = 1$) and purely diffused damage ($n_b = h_1/h_0$) as two limiting cases.

Evidently, parameter n_b must be related to the damage pattern. To achieve a proper energy regularization, we determine n_b based on the damage patterns of the element of interest as well as of its neighboring elements. We propose two descriptors $\delta_{\omega 1}$ and $\delta_{\omega 2}$. The first descriptor $\delta_{\omega 1}$ is concerned with the damage pattern in terms of the damage level of the element of interest relative to its adjacent elements, and the second descriptor $\delta_{\omega 2}$ is concerned with the damage pattern of the surrounding elements, which will be used to determine the effect of damage propagation.

To quantitively describe the damage pattern, we first identify the two adjacent finite elements denoted by m and n, whose positions relative to the element i are the most closely aligned with the principal vector $\vec{n}_e$, i.e. perpendicular to the cracking direction of element i (Fig. 4). We define the localization parameter $\delta_{\omega 1}$ for element i by

$$\delta_{\omega 1} = \left\langle 1 - \frac{\hat{\omega}_m + \hat{\omega}_n}{2\hat{\omega}_i} \right\rangle^{1/2} \tag{5}$$

where $\langle x \rangle = \max(x, 0)$, and $\hat{\omega}_i, \hat{\omega}_m, \hat{\omega}_n$ = representative damage levels of elements i, m, and n, respectively. Note that, when the structure is totally undamaged, we need to prescribe a particular value to $\delta_{\omega 1}$ instead of using Eq. 5, which will be discussed later.

The representative damage of element k is calculated by nonlocal averaging the damage values of the element itself and its adjacent two elements (elements $k-1$ and $k+1$) that are located closest to the principal vector of element k:

$$\hat{\omega}_k = \alpha_w \bar{\omega}_k + \frac{1-\alpha_w}{2}\left(\bar{\omega}_{k-1} + \bar{\omega}_{k+1}\right) \tag{6}$$

where $\bar{\omega}_r$ ($r = k, k+1, k-1$) denotes the damage level of element r, as calculated by averaging the damage values at all Gauss points of the element, and α_w is a constant that is less than 1. Based on Eq. 5, it is clear that $\delta_{\omega 1}$ is equal to 0 in the case of purely diffused damage. When the damage is fully localized into element i, $\delta_{\omega 1}$ reaches the maximum value:

$$\delta_{m1} = \langle 1.5 - 0.5\alpha_w^{-1} \rangle^{1/2} \tag{7}$$

Since $\delta_{m1} > 0$, constant α_w must be larger than 1/3. Here we choose $\alpha_w = 0.5$.

It is worthwhile to comment on the present definition of the representative damage variable. In deterministic analysis, it suffices to directly use the local damage value to calculate the localization parameter $\delta_{\omega 1}$ [13]. However, this is not the case for stochastic simulations. In stochastic FE analysis, the probability distribution of constitutive properties would cause some randomness in the stress and strain fields. Consequently, even if the material experiences diffused damage, the stochastic simulations would predict some mild variation across the local damage parameters of finite elements. If we use local damage parameters to determine the localization parameter, the model could predict a pattern of damage localization. This would lead to a reduction of the overall energy dissipation capacity of the element when the element size is larger than the size of the damage zone. This energy regularization would promote the premature damage localization process.

By employing the nonlocal averaging, the representative damage parameter is less affected by the variability of the stress field and damage distribution due to the stochasticity of the constitutive parameters. Therefore, the model can effectively mitigate the influence of the variation of local damage parameter on the prediction of the overall damage pattern.

The second descriptor $\delta_{\omega 2}$ is proposed to determine whether the damage of the current finite element is caused by the propagation of the localized damage in the adjacent element. We define $\delta_{\omega 2}$ for element i as:

$$\delta_{\omega 2} = \max_j \left[\delta_{\omega 1 j} \left(1 - |\vec{n}_e \cdot \vec{v}_{ij}|\right)^2 \right] \tag{8}$$

where $\delta_{\omega 1j}$ denotes the localization parameter $\delta_{\omega 1}$ of the neighboring element j, $\vec{n}_e$ is the principal vector of element i, and $\vec{v}_{ij}$ is the unit vector connecting the centroids of elements i and j. Eq. 8 indicates that $\delta_{\omega 2}$ of element i will attain its maximum value δ_{m2}, which equals to δ_{m1}, when one of its adjacent elements j exhibits a localized damage pattern and meanwhile the position of element j relative to element i aligns along the cracking direction of element i.

To develop an approximate expression for the number of active FPZs in the element, we consider the following limiting cases: 1) when $\delta_{\omega 1} = \delta_{m1}$ (fully localized damage in the current element), we have $n_b = 1$; 2) when $\delta_{\omega 2} = \delta_{m2}$ (propagation of fully localized damage into the current element), we have $n_b = 1$; 3) when $\delta_{\omega 1}$ is very small and yet $\delta_{\omega 2}$ is not too large, we have a diffused damage pattern in the current element and n_b approaches h_1/h_0. Based on these aforementioned limiting behaviors, we propose

$$n_b = 1 + \left(\frac{h_1}{h_0} - 1\right) \left\{1 - \left[\frac{\langle \delta_{\omega 1} - \delta_{t1} \rangle}{\delta_{m1} - \delta_{t1}}\right]^{\kappa}\right\} \left\{1 - \left[\frac{\langle \delta_{\omega 2} - \delta_{t2} \rangle}{\delta_{m2} - \delta_{t2}}\right]^{\lambda}\right\} \tag{9}$$

where κ, λ, δ_{t1}, δ_{t2} = constants. With a small number of parameters, Eq. 9 provides a flexible form for different transitional behaviors between the purely diffused and localized damage cases. Note that a similar functional form was also used in the recently developed energy regularization scheme for deterministic analysis [13]. Using this functional form for the stochastic case leads to a coherent model for both energy regularization and probabilistic modeling.

Eq. 9 indicates that, if both $\delta_{\omega 1}$ and $\delta_{\omega 2}$ are smaller than their respective threshold values δ_{t1}, δ_{t2}, we consider that the element experiences a fully diffused damage. These thresholds are used to further avoid the prediction of premature localization due to the effect of spatial distribution of random constitutive properties. Fig. 5 shows the relationship among n_b, $\delta_{\omega 1}$ and $\delta_{\omega 2}$.

To complete the formulation of the constitutive model, we consider the following free energy function Y for tension-dominated damage:

$$Y = \frac{1}{2} f(\omega) E \bar{\epsilon}^2 \tag{10}$$

$$\text{where} \quad \bar{\epsilon} = \sqrt{\sum_{k=1}^{3} \langle \epsilon_k \rangle^2} \tag{11}$$

where E = Young's modulus, $\bar{\epsilon}$ = equivalent strain defined in [26], ϵ_k = the principal values of the strain tensor. By substituting Eq. 10 into Eq. 3, we arrive at the following damage evolution equation:

$$\frac{\mathrm{d}f(\omega)}{\mathrm{d}\omega} = -\frac{2 n_b \bar{G}_f}{E h_1 \bar{\epsilon}^2} H(\bar{\epsilon} - \epsilon_0) H(\dot{\bar{\epsilon}}) \qquad (0 \le \omega < 1) \tag{12}$$

where $H(x)$ = Heaviside function, ϵ_0 = threshold strain, and $\dot{\bar{\epsilon}} = \mathrm{d}\bar{\epsilon}/\mathrm{d}t$. Eq. 12 indicates no damage growth when $\bar{\epsilon}$ is less than the threshold strain or the material experiences tensile unloading. Since $\max \omega = 1$, we require $\mathrm{d}f(\omega)/\mathrm{d}\omega = 0$ when $\omega = 1$.

To establish the relation between the damage variable and the deformation state, we employ the following damage function [13]

$$f(\omega) = \frac{1-\omega}{1-\eta\omega} \tag{13}$$

where η is a parameter which depends on the material properties as well as the energy regularization. To derive the expression of η, we consider the case of monotonic uniaxial tensile loading. Based on Eqs. 12 and 13, we obtain

$$\omega = \frac{1}{\eta} - \frac{\epsilon}{\eta}\sqrt{\frac{h_1 E(1-\eta)}{2n_b \bar{G}_f}} \tag{14}$$

where ϵ = uniaxial strain. Parameter η can then be calculated based on the fact that $\omega(\epsilon_0^+) = 0$. In this study, we choose $\epsilon_0 = f_t/E$, where f_t = tensile strength of the element. This indicates that, in monotonic tensile test, there is no stiffness degradation in the pre-peak region. This model leads to a linear softening behavior of the uniaxial tensile stress-strain curve.

Based on the aforementioned definition of ϵ_0, we express parameter η by

$$\eta = 1 - \frac{2n_b E \bar{G}_f}{h_1 f_t^2} \tag{15}$$

Combination of Eqs. 12, 13, and 15 completes the formulation of the constitutive model. The main feature of the model is its dependence on the damage pattern through parameter n_b. For each time increment, the tangential stiffness of the finite element is adjusted to be consistent with the prevailing damage pattern. This ensures the correct energy dissipation of the finite element during the evolution of the damage pattern.

4. Mechanism-Based Modeling of Probability Distributions of Constitutive Properties

The present model involves the following constitutive parameters: E = Young's modulus, ν = Poisson's ratio, f_t = tensile strength, $\bar{G}_f$ = average mode I fracture energy, and h_0 = FPZ width. In this study, we consider the tensile strength and fracture energy to be spatially random variables, which are mutually independent. The remaining parameters are treated to be deterministic. To model the spatial distribution of random variables, we generally need to know their probability distributions as well as the spatial correlation functions. For quasibrittle materials, the correlation length of random strength and fracture properties was estimated to be approximately similar to the width of the FPZ [14]. Since the focus of this study is on the case of mesh sizes that are larger than the FPZ width, we can ignore the spatial correlations of tensile strength and fracture energy. What remains to be determined are the probability distribution functions of tensile strength f_t and average fracture energy $\bar{G}_f$.

4.1 Probability distribution of average fracture energy

Based on Eq. 4, $\bar{G}_f$ represents the average of the fracture energies of all the FPZs formed in the element. It is evident that the probability distribution of $\bar{G}_f$ is governed by the probability distribution of the fracture energy G_f associated with an individual FPZ, which is considered as a material property. In this study, we consider the fracture energy G_f follows a Gaussian distribution of a mean value μ_G and coefficient of variation (CoV) w_G. The choice of the Gaussian distribution is motivated by the fact that the fracture energy associated with a macrocrack can be considered as the sum of the energy dissipations of all microcracks inside the FPZ, which are intrinsically random. It is admitted that one issue with the Gaussian distribution for fracture energy is that it permits negative values. However, this issue is not important for most stochastic analyses since the chance of sampling a negative fracture energy is extremely low.

As mentioned earlier, we consider the fracture energies of FPZs to be statistically independent. Since the fracture energy of a single FPZ is taken as Gaussian, we can conclude that the probability distribution of the average fracture energy $\bar{G}_f$ must also be Gaussian. The mean and CoV of $\bar{G}_f$ can be written by

$$\mu_{\bar{G}} = \mu_G \tag{16}$$

$$w_{\bar{G}} = \frac{w_G}{n_b}\sqrt{k_b - 1 + (n_b + 1 - k_b)^2} \tag{17}$$

It is clear that the mean of average fracture energy is not affected by the damage pattern but the CoV is. Therefore, as the damage pattern evolves during the loading process, the probability distribution of the average fracture energy could change. Furthermore, it is noted that, depending on the damage pattern, the CoV of the average fracture energy could vary with the mesh size. For instance, if the element exhibits a diffused damage pattern, the CoV of $\bar{G}_f$ would decrease significantly with an increasing mesh size.

4.2 Probability distribution of tensile strength

To derive the probability distribution of tensile strength, we consider a damage zone of width h_d formed in the element (Fig. 3b). Note that this damage zone could contain several FPZs if the damage is not fully localized. In deterministic analysis, what matters only is the size of the damage zone, and the tensile strength of the element is equal to that of the damage zone. This is why we only consider energy regularization of the constitutive model, where the tensile strength of the element is set to be the material's tensile strength. However, this is not the case for stochastic analysis. Here we need to take into account the fact that the location of the damage zone is intrinsically random. In a given element, the actual damage zone will occur at the location where the tensile strength is minimum. Once one damage zone is formed and undergoes softening damage, the remaining part of the element experiences elastic unloading. Therefore, the tensile strength of the element is equal to the minimum of the tensile strengths of all the potential damage zones.

Based on the foregoing discussion, the probability distribution of f_t can be described by a weakest-link model. Since the size of the damage zone is considered to be larger than the autocorrelation length of the random field of tensile strength, the cdf of f_t can be calculated using the joint probability theorem, i.e.:

$$P_t(x) = 1 - [1 - P_1(x)]^{n_f} \tag{18}$$

where n_f = number of potential damage zones in the element, and $P_1(x)$ is the cdf of tensile strength of each damage zone. Depending on the damage pattern, the damage zone may consist of several FPZs. Therefore, the cdf of tensile strength of a damage zone, $P_1(x)$, cannot be considered as a material property. Instead, it should be derived from the cdf $P_0(x)$ of tensile strength of a single FPZ, a basic material property.

In a series of recent studies [8, 5, 20, 4], a mechanistic model was developed for the strength distribution of FPZ. Based on the atomistic fracture mechanics and a statistical multiscale transition model, it was shown that $P_0(x)$ can be described by a Gaussian distribution onto which a power-law tail is grafted on its left, i.e.:

$$P_0(x) = \begin{cases} 1 - \exp(-\langle x/s_0\rangle^{m_0}) \approx \langle x/s_0\rangle^{m_0} & (x \le x_{g0}) \quad (19a) \\ P_{g0} + \dfrac{r_{f0}}{\delta_0\sqrt{2\pi}}\displaystyle\int_{x_{g0}}^{x} e^{-(x'-\mu_0)^2/2\delta_0^2}\mathrm{d}x' & (x > x_{g0}) \quad (19b) \end{cases}$$

where m_0 and s_0 are the Weibull modulus and scale parameter of the Weibull tail, respectively, μ_0 and δ_0 are the mean and standard deviation of the Gaussian core if considered extended to $-\infty$; r_{f0} is a scaling parameter required to normalize the grafted cdf such that $P_1(\infty) = 1$, x_{g0} = grafting stress, and $P_{g0} = (x_{g0}/s_0)^{m_0}$ = grafting probability. We impose the continuity of the probability density function (pdf) at the grafting point, i.e. $[\mathrm{d}P_1/\mathrm{d}x]_{x_{g0}^+} = [\mathrm{d}P_1/\mathrm{d}x]_{x_{g0}^-}$.

Now consider the damage zone contains n_b number of FPZs. Since the damage zone is featured by a diffused damage pattern, it is reasonable to consider the strength of the damage zone as the average of the random strengths of all the FPZs inside it. It has been shown that, if the strength of one FPZ follows a Gauss-Weibull grafted distribution, the average of the FPZ strengths could also be described by the same type of distribution (Eqs. 19a and 19b) but its parameters carry different values [21]. The grafted distribution $P_1(x)$ of the average tensile strength can be defined by the following four parameters:

$$\mu_1 = \mu_0 \tag{20}$$

$$w_1 = \frac{\delta_0}{\mu_0 n_b}\left[k_b - 1 + (n_b + 1 - k_b)^2\right]^{1/2} \tag{21}$$

$$m_1 = k_b m_0 \tag{22}$$

$$P_{g1} = (P_{g0}/k_b)^{k_b} \tag{23}$$

where μ_1, w_1 = mean and CoV of the Gaussian core of the grafted distribution function $P_1(x)$, respectively, m_1 = Weibull modulus of the left tail of $P_1(x)$, and P_{g1} = grafting probability at which the Weibull tail of $P_1(x)$ terminates.

What remains to be defined is the number of potential damage zones, n_f. We note two different scenarios: 1) damage initiates and develops in the current element, and 2) the damage of the current element is caused by the propagation of a localized damage from a neighboring element. These two scenarios have different implications for stochastic analysis. In the first scenario, the location of the damage zone is random, which is dictated by the minimum tensile strength of the potential damage zones. Therefore, we have $n_f = h_1/n_b h_0$. In the second scenario, the location of the damage zone is no longer random, but is determined by the damage zone that was formed in the neighboring element. In this case, we have $n_f = 1$. Here we use the second localization descriptor $\delta_{\omega 2}$ to differentiate these two scenarios and express n_f by

$$n_f = \frac{h_1}{n_b h_0} + \left(1 - \frac{h_1}{n_b h_0}\right)\left[\frac{\langle \delta_{\omega 2} - \delta_{t2}\rangle}{\delta_{m2} - \delta_{t2}}\right]^{\lambda} \tag{24}$$

Eq. 24 indicates that, in the absence of propagating damage, the number of potential damage zones at damage initiation is equal to $h_1/n_b h_0$. As the effect of propagating damage becomes pronounced, the value of n_f would approach 1.

4.3 Sampling of tensile strength and average fracture energy

Based on the foregoing discussion, it is clear that the cdfs of tensile strength f_t and average fracture energy $\bar{G}_f$ are intimately related to the prevailing damage pattern. Consequently, the formulations of these cdfs are coherent with the energy regularization of the constitutive law (Eq. 3). In general, the damage pattern of the structure could evolve during the loading process. A common example is the transition from a diffused damage pattern to the initiation and propagation of localized damage. In the present framework, this implies that the cdf of tensile strength and average fracture energy would vary during the loading. In the FE simulation, this is manifested by the adjustment of the tangential stiffness tensor for every time step.

In the numerical implementation, we first generate two independent uniformly distributed random variables u_1, u_2, which range from 0 to 1, for each element. For fixed values of u_1 and u_2, we calculate the corresponding tensile strength and average fracture energy by

$$\bar{G}_f = \mathcal{N}^{-1}(u_1) \tag{25}$$

$$f_t = P_t^{-1}(u_2) \tag{26}$$

where $\mathcal{N}(x)$ = Gaussian distribution function of the average fracture energy, which has a mean of $\mu_{\bar{G}}$ and a CoV of $w_{\bar{G}}$, and $P_t(x)$ = cdf of tensile strength (Eq. 18).

As mentioned earlier, here we treat strength and fracture energy of each FPZ to be independent random variables, which is a simplification. It may be expected that the random tensile strength and fracture energy of quasibrittle materials could exhibit some statistical correlation. However, this correlation is not well understood yet, and very limited experimental data is available. It is noted that the present model can be extended to model correlated fracture energy and tensile strength. In this case, we need to first derive the correlation between the average fracture energy $\bar{G}_f$ and tensile strength f_t of the finite element based on the correlation of the input fracture energy and tensile strength of one FPZ. The correlated $\bar{G}_f$ and f_t can then be sampled by using the Nataf transformation [15].

Since the cdfs of the tensile strength and average fracture energy may vary due to the evolving damage pattern, Eqs. 25 and 26 indicate that the sampled $\bar{G}_f$ and f_t could change during each time step, which directly affects the tangential stiffness tensor. Here it should be emphasized that the input basic material properties are the probability distributions of fracture energy and strength associated with a single FPZ. The tensile strength f_t and average fracture energy $\bar{G}_f$ are not material properties, but represent the behavior of the finite element. They depend on the damage mechanism and therefore could change over the loading process.

We note that the present formulation of the cdfs of tensile strength and average fracture energy relies on the localization parameters $\delta_{\omega 1}$ and $\delta_{\omega 2}$. Both parameters are calculated based on the damage variable ω. Therefore, it is important to discuss the initial values of $\delta_{\omega 1}$ and $\delta_{\omega 2}$ before damage initiates. In this study, we consider $\delta_{\omega 1} = \delta_{m1}$, and $\delta_{\omega 2} = 0$ as the initial values. The reason for $\delta_{\omega 2} = 0$ is obvious since there is no propagating damage at the initial undamaged state. To determine the initial value of $\delta_{\omega 1}$, we consider the earlier 1D analysis of the uniaxial tension specimen (Sec. 2). It is obvious that, in this simple example where damage localization occurs right away as damage initiates, we must set initial value of $\delta_{\omega 1}$ to δ_{m1}. In a general case, damage localization may not occur immediately. However, choosing $\delta_{\omega 1} = \delta_{m1}$ as an initial condition has a minimal effect on the simulation results. This is because, as soon as damage initiates, the model would predict the correct prevailing damage pattern, and immediately adjust the localization parameters.

5. Numerical Study

5.1 Description of Analysis

The present model is now applied to simulate the probabilistic failure behaviors of three-point and four-point bend specimens. The simulations are performed in an open-source FEM software (OOFEM) [28]. For the three-point bending test, the beam has in-plane dimensions of 7.5 mm (length) × 2.5 mm (depth). Both notched and unnotched specimens are considered (Fig. 6a and b). For notched specimen, the notch depth is 50% of the beam depth, and the notch width is equal to $h_0/2$ (Fig. 6b), where h_0 = crack band width. The four point bend beam has a total span of 11.25 mm and depth of 2.5 mm. The span between the two loading points is 7.5 mm. Only the unnotched beam is considered for the four-point bending test (Fig. 6c). All specimens are modeled by 2D plane stress elements of thickness of h_0. To avoid premature compressive failure, the finite elements in the vicinity of the loading points and supports are modeled to behave elastically.

We consider the beams to be made of a dense alumina ceramic with Young's modulus $E = 370$ GPa and Poisson's ratio $\nu = 0.24$. The width of the FPZ, h_0, is set to be 37.5 μm, which is a few times the average grain size of the material. The input probability distribution of the fracture energy of a single FPZ follows a Gaussian cdf with mean $\mu_G = 50$ J/m^2 and CoV $\omega_G = 0.15$. The tensile strength of the

FPZ follows a Gauss-Weibull grafted distribution (Eqs. 19a and 19b) with the following parameters: $\mu_0 = 200$ MPa, $\delta_0 = 30$ MPa, $m_0 = 30$, and $P_{g0} = 5 \times 10^{-3}$. Fig. 6d shows the mean uniaxial tensile stress-strain curve of the material.

In the simulation, the specimen is loaded in the displacement-controlled mode, from which the entire load-displacement curve is obtained. The stochastic simulations yield the mean and standard deviation of the peak load, denoted by $\bar{P}_m$ and δ_P, which are the two most critical parameters for reliability-based design. The main objective of this numerical analysis is to evaluate the performance of the present model for mitigating the spurious mesh sensitivity in stochastic FE analysis, and also to investigate the role of mechanism-based modeling of the probability distributions of fracture and strength properties. To this end, we consider the following three probabilistic models for comparison purposes:

I. The present model, where the tensile strength and fracture energy are sampled from the distributions of Eqs. 25 and 26 respectively, which are constantly updated based on the prevailing damage pattern through parameters n_f and n_b.

II. The weakest-link model for the tensile strength, i.e. $P_t = 1 - (1 - P_0)^{h_1/h_0}$ where P_0 is the tensile strength distribution of one FPZ. The weakest-link model is based on the assumption of structural failure with initiation of damage localization, and therefore the average fracture energy is considered to be the same as the fracture energy of a single FPZ, which follows a Gaussian cdf $\mathcal{N}(\mu_G, w_G)$.

III. The constant distribution model, where the material properties of tensile strength and fracture energy are sampled from a Gauss-Weibull grafted cdf $P_t = P_0(\mu_0, m_0, \delta_0, P_{g0})$, and a Gaussian distribution $\mathcal{N}(\mu_G, w_G)$, respectively. In this model, the statistical parameters do not depend on the element size.

In all of the aforementioned models, we implement the energy regularization scheme described in Sec. 3 so that the constitutive model is regularized to ensure the correct energy dissipation. Therefore, the resulting mesh dependence of FE simulations can be attributed to the treatment of the probability distributions of constitutive properties, a key point of this study.

In the simulation, all beams are discretized by a uniform mesh consisting of quadrilateral bilinear elements with full Gauss integration. To investigate the mesh dependence, three different mesh sizes are considered: the reference case with dimensions of finite elements $h_x = h_0$ and $h_y = h_0$, where subscripts x, y, denote the directions of the beam span and depth respectively, and two other coarser meshes with $h_x = 2h_0$ and $h_x = 4h_0$ whereas h_y is kept to be h_0. The mesh lines are aligned approximately with the direction of overall damage growth. Therefore, the element size h_1 along the principal direction is approximately equal to h_x. For the notched beams, the element at the notch tip is trapezoidal, with the upper base being h_x and the lower base being the notch width.

For each specimen geometry, we perform a large number of stochastic simulations to obtain converged results of the mean and standard deviation of the peak load. For each of the three models, the parameters of the energy regularization function $(\delta_{t1}, \delta_{t2}, \kappa, \lambda)$ are calibrated to suppress the mesh dependence of the mean peak load $\bar{P}_m$ of the unnotched three-point bend beams. The choice of this calibration case is based on the fact that, as compared to the other geometries, the unnotched three-point bend beam exhibits a more complicated failure mechanism transitioning from diffused damage to localized damage. Once calibrated for a given material and modeling approach, the values of parameters $\delta_{t1}, \delta_{t2}, \kappa$, and λ are kept fixed for other different structure geometries and loading configurations.

5.2 Unnotched beams under three-point bending

In this section we investigate the simulated peak load of unnotched beams under three-point bending. Figs. 7a and b present the mean and standard deviation of the peak load calculated from 500 stochastic simulations, where the random tensile strength and average fracture energy are sampled using models I–III. As mentioned earlier, parameters δ_{t1}, δ_{t2}, κ, and λ are calibrated separately for each model such that the mesh dependence of the mean response of the unnotched three-point bend beams is mitigated, as shown in Fig. 7a. In the calibration of each model, we use the mean peak load calculated for $h_x = h_0$ as the benchmark solution. The model parameters are then determined by minimizing the mean squared deviation (MSD) of the mean peak loads calculated for $h_x = 2h_0$ and $h_x = 4h_0$. Fig. 7a shows the predicted mean peak loads for different mesh sizes by using the three models. The MSDs for models I-III are 2.1%, 2.9%, 1.6%, respectively, and the optimum values of the model parameters are found to be $\delta_{t1} = \delta_{t2} = 0$, $\kappa = \lambda = 1$ for model I and model III, whereas $\delta_{t1} = \delta_{t2} = 0.7$, $\kappa = \lambda = 1$ for model II.

Based on Fig. 7b, we observe that the present model gives the best result with a maximum difference of 11% in the predicted standard deviation between the reference mesh and the coarse mesh. Model III yields a maximum difference of 16%, and model II results in the worst performance with a maximum difference of 54%. The mesh dependence of the simulated standard deviation δ_P can be understood based on the failure mechanism of the beam. The randomness of material properties naturally causes randomness in the number of damaged elements as well as in the location of macrocrack initiation. However, the randomness does not affect the prevailing damage mechanism when the peak load is reached. At the peak load, the beam contains a microcracking zone, from which a macrocrack initiates (Fig. 8). Inside this zone, the elements experience more of a diffused damage pattern rather than localized damage. Fig. 8 further shows that the size of the microcracking zone is mildly affected by the mesh size.

The peak load is closely related to the energy dissipation of all the elements in the diffused microcracking zone. Therefore, the statistics of the overall peak load reflects an averaging effect of the random properties of the finite elements inside the zone. Since the size of the microcracking zone is approximately constant, a coarser mesh implies a smaller number of finite elements in the zone. It is expected that, in order to attain mesh-independent statistics of the maximum load, we must change the randomness of the constitutive properties of the finite elements as the mesh size varies.

The present model captures the averaging effect because the probability distributions of the strength and fracture properties depend on the localization parameters, which quantify the actual damage pattern of the element. For the elements in the diffused damage zone, the present model predicts small values of $\delta_{\omega 1}$ and $\delta_{\omega 2}$, and therefore the cdfs of tensile strength f_t and average fracture energy $\bar{G}_f$ are dependent on the mesh size. The CoVs of both tensile strength and average fracture energy decrease with an increasing mesh size. This mesh dependence of random properties helps reduce the mesh dependence of the calculated statistics of the peak load.

For model III, where the input cdfs of f_t and $\bar{G}_f$ are made mesh-size independent, the predicted standard deviation δ_P shows a more pronounced mesh dependence than that predicted by the present model. The difference in the results predicted by the present model and model III is not significant over the range of the mesh sizes considered in this study. However, this difference is expected to be more pronounced if we use a larger mesh size. It should also be pointed out that, though model III is convenient to use, it is only applicable to the case of propagation of localized damage.

In this numerical example, the most significant mesh dependence of δ_P is found in model II, where the cdf of tensile strength is modeled by the weakest-link model regardless of the damage pattern. The weakest-link model corresponds to the scenario of fully localized damage, which is clearly not the case in the present simulation. The weakest-link model implies a significant decrease in the mean tensile strength with an increasing mesh size, which leads to a decrease in the mean peak load as the mesh size increases. In order to mitigate this mesh dependence, we increase significantly the values of δ_{t1} and δ_{t2}. This implies that, for a wide range of $\delta_{\omega 1}$ and $\delta_{\omega 2}$, the model would predict a fully diffused damage pattern and therefore a maximum value of n_b. In this case, the energy regularization scheme gives the maximum increase in the energy dissipation with an increasing mesh size, which compensates the decrease in the mean tensile strength. Therefore, the model overestimates n_b. By using a mesh-size independent cdf of the average fracture energy, the model grossly over-predicts the standard deviation of the peak load.

The foregoing analysis indicates that the performance of models II and III is largely affected by the prevailing damage mechanism. In the present case, the material is not sufficiently brittle and therefore a microcracking zone of considerable size is formed prior to the peak load. This makes model III outperform model II. To further demonstrate the role of damage mechanism in the modeling of the probability distributions of constitutive properties, we simulate the same beam but with a reduced mean fracture energy $\mu_G = 15$ J/m^2, whereas the other statistical properties of strength and fracture energy are kept the same. In this case, the material is more brittle, and at the peak load the beam experiences a more localized damage. When changing the material properties, we recalibrate the model parameters to mitigate the mesh dependence on the mean behavior, which gives $\delta_{t1} = \delta_{t2} = 0.6$, $\kappa = 1$, $\lambda = 1$ for the proposed model, $\delta_{t1} = \delta_{t2} = 0.7$, $\kappa = 1$, $\lambda = 1$ for model II, and $\delta_{t1} = \delta_{t2} = 0$, $\kappa = 1$, $\lambda = 1$ for model III.

Fig. 9 presents the mesh size dependence of the output mean and standard deviation of peak load for all three models. It is seen that, for all three models, the mesh dependence of the mean behavior can be mitigated by calibration of the model parameters. For the output standard deviation δ_P, now the present model and model II show mild mesh dependence, and model III yields strong mesh dependence. The performances of models II and III in this case are opposite to what we observed in the previous case with a higher mean fracture energy. This difference is due to the fact that in this case the beam shows a more localized damage pattern, which favors the weakest-link model of tensile strength. The foregoing analysis indicates that models II and III lack of robustness since they are only suitable for some particular damage patterns. On the contrary, the present model gives a consistent performance for both cases because the formulation of the cdfs is tied to the damage pattern.

5.3 Notched beam under three-point bending

The second numerical study is concerned with a pre-notched beam under three-point bending. The material and size of the beam are the same as that used in the first example ($\mu_G = 50$ J/m^2) except that now the beam has a pre-existing notch at the midspan, and the notch depth is 50% of the beam depth. The presence of the notch causes a significant stress concentration and therefore the location of damage initiation is almost deterministic. Evidently, damage localization has occurred at the peak load. Therefore, it is expected that the energy regularization will essentially be the same as the crack band model [7].

For the notched beam, there is a FPZ formed at the notch tip when the peak load is attained. In the present numerical model, the formation of FPZ is characterized by sequential damage of a column of elements above the notch tip. Therefore, the primary failure mechanism of this specimen is the propagation of localized damage. It is well expected that the present model and model III would yield a good result, whereas the simulation by model II would exhibit pronounced mesh dependence.

Fig. 10 shows the predicted mean and standard deviation of the peak load for different mesh sizes. It is seen that the proposed model and model III give very similar results, which show weak mesh dependence. This is because, for the aforementioned failure mechanism, the present model essentially converges to model III except for the strength cdf of the element right above the notch tip. Since the FPZ consists of many elements, the difference in strength cdf of one element does not have a significant effect on the statistics of the overall peak load.

The simulation by model II yields pronounced mesh dependence in the predictions of both mean and standard deviation of the peak load. The simulation by model II shows that the mean peak load decreases considerably with an increasing mesh size. This behavior is due to the fact that the weakest-link model of the tensile strength implies a decreasing mean strength with an increasing mesh size. As the mesh size increases, the predicted standard deviation δ_P first increases and then shows a significant decrease. To explain this non-monotonic behavior, we first note that, due to the spatial distribution of random strength and fracture energy, it is possible that elements next to the crack ligament experience slight damage. As mentioned earlier, the calibrated thresholds δ_{t1}, δ_{t2} for model II are very close to their maximum values. Consequently, the model erroneously predicts a diffused damage pattern. Similar to the case of unnotched beams, this leads to an increase in the standard deviation of the peak load. On the other hand, model II indicates that the standard deviation of the tensile strength decreases considerably with an increasing mesh size. This causes the standard deviation of the peak load to decrease as the mesh size increases. The observed mesh dependence of δ_P is a consequence of the competition of the aforementioned two effects. For the case of $h_x = 2h_0$, the first effect is dominant while the second effect overrides the first effect for the case of $h_x = 4h_0$.

To further reinforce the foregoing discussion, we perform the simulation by using model II with smaller thresholds $\delta_{t1} = \delta_{t2} = 0.6$. Fig. 11 shows the simulation result together with the aforementioned model II prediction. It is seen that both the mean and standard deviation of the peak load simulated by using $\delta_{t1} = \delta_{t2} = 0.6$ are lower than those simulated by using $\delta_{t1} = \delta_{t2} = 0.7$. Meanwhile, with decreased values of δ_{t1} and δ_{t2}, both the mean and standard deviation of the peak load decrease significantly with an increasing mesh size. These observations are attributed to the fact that, by decreasing the thresholds, the model correctly predicts the localized damage pattern (i.e. $n_b = 1$). The observed mesh dependence on peak load is solely due to the mesh dependence of the statistics of tensile strength.

5.4 Unnotched beam under four-point bending

The last numerical example considers an unnotched beam under four-point bending. In the elastic range, the bending moment is constant between the two loading points. Therefore, we expect that, prior to the formation of localized macrocracks, the specimen would experience a more diffused damage pattern as compared to the case of three-point bending. The material properties are the same as these used in the first numerical example. In the simulation, the beam is loaded through two contacts of a rigid plate, which is pushed down in a displacement control mode at its mid-point (Fig. 6c). For each sampling model (models I-III), the mean $\bar{P}_m$ and standard deviation δ_P of the peak load are calculated through 400 stochastic simulations.

Figs. 12a and b present the simulated mean and standard deviation of peak load of the beam with respect to the element size h_x, for all three models. It is seen that all models are able to effectively mitigate the mean size effect. For the mesh dependence of δ_P, it can be seen that the present model is able to provide an almost mesh-insensitive result. The prediction by Model III shows a mild mesh dependence with a maximum deviation of 7% between the reference mesh and the coarse mesh, which is lower than the case of three-point bending. This can be attributed to the fact that in four-point bending the beam first exhibits a large microcracking zone, and subsequently there are several macrocracks initiating from this zone (Fig. 13). Therefore, the statistics of the peak load is governed by the energy dissipation of the microcracking zone as well as the formation of the macrocracks. Since the sampling method of model III is suitable to describe the damage propagation mechanism, it results in weaker mesh dependence than the case of three-point bending of unnotched beams, in which only one macrocrack initiates from the microcracking zone. Nevertheless, due to the use of a mesh-independent cdf of the average fracture energy, model III over-predicts the randomness of the energy dissipation of the microcracking zone, which is responsible for the observed increasing trend of the standard deviation δ_P over the increasing mesh size. It is expected that the mesh dependence would become more pronounced if we use a larger mesh size.

The prediction by model II still suffers strong mesh dependence, though milder than the first example of three-point bend beam. This is because, under four point bending, the beam experiences a more diffused damage pattern before localized damage initiates. Therefore, in this case the calibrated parameters of model II do not grossly over-predict the value of n_b as it does in the case of three-point bending. However, since the input cdf of the average fracture energy is mesh independent, the predicted standard deviation δ_P consistently increases with the mesh size.

5.5 Further discussion

The analysis of uniaxial tension specimen in Sec. 2 features a case of purely localized damage occurring at a random location. This case demonstrates the deficiency of using a mesh-independent strength cdf (i.e. model III). In the numerical study, the unnotched three-point bend and four-point bend beams exhibit a transition from diffused microcracking to formation and propagation of localized damage. This transition is largely affected by the brittleness of the material and the structure geometry. The notched specimen experiences localized damage right away at a predefined location. It is seen that, with one set of model parameters calibrated to suppress mesh dependence of the mean behavior for one geometry, the present model can effectively mitigate the mesh dependence on both the mean and standard deviation of the peak loads for other different structure geometries. By contrast, models II and III perform well only for some particular cases.

The probabilistic model of constitutive properties has a profound influence on the mesh dependence of the stochastic FE simulations. The selected probability distributions of strength and fracture properties reflect some certain damage mechanism. The mesh dependence of FE simulation can be attributed to the mismatch between the actual damage pattern in the structure and that implied by the probabilistic distributions. By using the fixed forms of probability distribution functions, the stochastic model severely lacks robustness since it is only applicable to a certain structure geometry and loading configuration. Therefore, it is crucial to sample the random constitutive properties from the cdfs that correspond to the prevailing damage pattern, which is the key feature of the present model. This feature makes the model applicable to different structure geometries exhibiting different damage mechanisms.

The foregoing discussion also indicates that, to validate a stochastic computational model even for a single failure mode (e.g. tensile failure), one would need histogram testing of specimens of different geometries featuring different damage patterns. Using specimens of one geometry is not sufficient to examine the validity of probabilistic distribution models of the constitutive parameters. Such a partial validation could severely limit the robustness of stochastic model.

In this study, we limit our attention to the case where the mesh size is larger than the spatial correlation length of the random constitutive properties, and therefore the spatial correlation is ignored. In a more general setting, we may model the spatial randomness of the constitutive properties as continuous random fields [34, 33, 12]. In stochastic FE simulations, the essential step is to map the continuous random fields to the finite element mesh. The mapping algorithm greatly affects the statistics of the constitutive properties of the finite element mesh. The results of the present study indicate that this mapping must be consistent with the prevailing damage pattern of the element, which is essential for suppressing the mesh dependence of the simulation results. In fact, the present model represents this mapping algorithm in a limiting case, where the mesh size is sufficiently large so that the correlation structure of the random field is ignored. A general mechanistic mapping algorithm will need to be developed to cover the case of small mesh sizes.

6. Conclusions

- Stochastic FE simulations of quasibrittle structures can exhibit strong mesh dependence of the statistics of structural response. To mitigate this mesh dependence, it is essential to consider two aspects: 1) energy regularization of the constitutive model, and 2) mechanism-based modeling of the probability distributions of the constitutive properties. These two considerations stem from the viewpoint that each finite element is regarded as a material element of finite size. Therefore, in FE simulations the constitutive model does not represent the property of a material point, but the behavior of a finite-size material element.
- Two localization parameters are proposed to describe the damage patterns of the finite element. These parameters are used to formulate the energy regularization scheme and the probability distribution functions of the strength and average fracture energy of the element. Consequently,

the energy regularization and sampling of random strength and fracture energy are governed by the prevailing damage pattern, which could evolve during the loading process. This results in the adjustment of the tangential stiffness tensor at each time increment in the FE simulation. The present model is applicable to different damage mechanisms, which include purely localized damage, purely diffused damage, as well as the transition from diffused damage to localized damage.
- The numerical analysis of the statistics of load capacities of different structures demonstrates the critical role of consideration of the damage mechanism in the sampling of the random constitutive properties. By deriving the probability distributions of constitutive properties based on the damage mechanism, the present model is able to effectively mitigate the mesh dependence in stochastic simulations of structures of different geometries, which feature different failure processes. On the contrary, if a fixed set of probability distribution functions is used, the stochastic computational model would be applicable only to certain structural geometries and loading scenarios, where the damage mechanism corresponds to the assumed probability distributions of the constitutive properties.

Acknowledgment: J.-L. Le and A. Gorgogianni acknowledge the financial support provided by the Nuclear Engineering University Program of the Department of Energy under grant DE-NE0008785. J. Eliáš acknowledges the financial support provided by the Czech Science Foundation under project No. GA19-12197S.

References

[1] B. Bahmani, R. Abedi, and P. L. Clarke. A stochastic bulk damage model based on Mohr-Coulomb failure criterion for dynamic rock fracture. *Appl. Sci.*, 9(5):830, 2019.

[2] Z. P. Bažant. Instability, ductility, and size effect in strain-softening concrete. *J. Engrg. Mech. Div., ASCE*, 102, EM2:331–44, 1976.

[3] Z. P. Bažant and L. Cedolin. *Stability of Structures: Elastic, Inelastic, Fracture and Damage Theories.* Oxford University Press, New York, 1991.

[4] Z. P. Bažant and J.-L. Le. *Probabilistic Mechanics of Quasibrittle Structures: Strength, Lifetime, and Size Effect.* Cambridge University Press, Cambridge, U.K., 2017.

[5] Z. P. Bažant, J.-L. Le, and M. Z. Bazant. Scaling of strength and lifetime distributions of quasibrittle structures based on atomistic fracture mechanics. *Proc. Nat'l. Acad. Sci., USA*, 106:11484–11489, 2009.

[6] Z. P. Bažant, J.-L. Le, and C. G. Hoover. Nonlocal boundary layer model: Overcoming boundary condition problems in strength statistics and fracture analysis of quasibrittle materials. In *Fracture Mechanics of Concrete and Concrete Structures—Recent Advances in Fracture Mechanics of Concrete.*, pages 135–43, Jeju, Korea, 2010.

[7] Z. P. Bažant and B.-H. Oh. Crack band theory for fracture of concrete. *Mater. Struc.*, 16:155–77, 1983.

[8] Z. P. Bažant and S. D. Pang. Activation energy based extreme value statistics and size effect in brittle and quasibrittle fracture. *J. Mech. Phys. Solids*, 55:91–131, 2007.

[9] Z. P. Bažant and J. Planas. *Fracture and Size Effect in Concrete and Other Quasibrittle Materials.* CRC Press, Boca Raton, FL, 1998.

[10] Z. P. Bažant and M. Jirásek. Nonlocal integral formulations of plasticity and damage: Survey of progress. *ASCE J. Eng. Mech.*, 128(11):1119–1149, 2002.

[11] N. P. Daphalapurkar, K.T. Ramesh, L. Graham-Brady, and J.-F. Molinari. Predicting variability in the dynamic failure strength of brittle materials considering pre-existing flaws. *J. Mech. Phys. Solids*, 59:297–319, 2011.

[12] J. Eliáš and M. Vořechovský. Fracture in random quasibrittle media: I. Discrete mesoscale simulations of load capacity and fracture process zone. *Eng. Fract. Mech.*, 235:107160, 2020.

[13] A. Gorgogianni, J. Eliáš, and J.-L. Le. Mechanism-Based Energy Regularization in Computational Modeling of Quasibrittle Fracture. *ASME J. Appl. Mech.*, 87(9), 2020.

[14] P. Grassl and Z. P. Bažant. Random lattice-particle simulation of statistical size effect in quasi-brittle structures failing at crack initiation. *J. Engrg. Mech., ASCE*, 135(2):85–92, 2009.

[15] A. Haldar and S. Mahadevan. *Probability, Reliability, and Statistical Methods in Engineering Design*. Wiley, New York, 2000.

[16] M. Jirásek. Mathematical analysis of strain localization. *Revue Européenne de Génie Civil*, 11:977–991, 2007.

[17] M. Jirásek and M. Bauer. Numerical aspects of the crack band approach. *Computers and Structures*, 110-111:60–78, 2012.

[18] A. Krayani, G. Pijaudier-Cabot, and F. Dufour. Boundary effect on weight function in nonlocal damage model. *Eng. Fract. Mech.*, 76(14):2217–2231, 2009.

[19] J.-L. Le. Size effect on reliability indices and safety factors of quasibrittle structures. *Struct. Saf.*, 52:20–8, 2015.

[20] J.-L. Le, Z. P. Bažant, and M. Z. Bazant. Unified nano-mechanics based probabilistic theory of quasibrittle and brittle structures: I. strength, crack growth, lifetime and scaling. *J. Mech. Phys. Solids*, 59:1291–1321, 2011.

[21] J.-L. Le, J. Eliáš, A. Gorgogianni, J. Vievering, and J. Květon. Rate-dependent scaling of dynamic tensile strength of quasibrittle structures. *ASME J. Appl. Mech.*, 85(2):021003, 2018.

[22] J.-L. Le and J. Eliáš. A probabilistic crack band model for quasibrittle fracture. *ASME J. Appl. Mech.*, 83(5):051005, 2016.

[23] R. B. Leavy, R. M. Brannon, and O. E. Strack. The use of sphere indentation experiments to characterize ceramic damage models. *Int. J. Appl. Cer. Tech.*, 7(5):606–615, 2010.

[24] W. Luo and Z. P. Bažant. Fishnet statistics for probabilistic strength and scaling of nacreous imbricated lamellar materials. *J. Mech. Phys. Solids*, 109:264–287, 2017.

[25] W. Luo and Z. P. Bažant. Fishnet statistical size effect on strength of materials with nacreous microstructure. *ASME J. Appl. Mech.*, 86(8), 2019.

[26] J. Mazars. *Application de la mécanique de l'endommagement au comportement non linéaire et à la rupture du béton de structure*. PhD thesis, University of Paris VI, Paris, France, 1984.

[27] H. W. Meyer Jr. and R. M. Brannon. A model for statistical variation of fracture properties in a continuum mechanics code. *Int. J. Impact Engrg.*, 42:48–58, 2012.

[28] B. Patzák. OOFEM - An object-oriented simulation tool for advanced modeling of materials and structures. *Acta Polytech.*, 52(6):59–66, 2012.

[29] R. H. J. Peerlings, R. de Borst, W. A. M. Brekelmans, and J. H. P. de Vree. Gradient-enhanced damage for quasi-brittle materials. *Int. J. Numer. Methods in Eng.*, 39:3391–3403, 1996.

[30] G. Pijaudier-Cabot and Z. P. Bažant. Nonlocal damage theory. *J. Eng. Mech., ASCE*, 113:1512–1533, 1987.

[31] E. Rizzi, I. Carol, and K. Willam. Localization analysis of elastic degradation with application to scalar damage. *J. Engrg. Mech., ASCE*, 121(4):541–554, 1995.

[32] J. W. Rudnicki and J. R. Rice. Conditions for the localization of deformation in pressure-sensitive dilatant materials. *J. Mech. Phys. Solids*, 23:371–394, 1975.

[33] E. Syroka-Korol, J. Tejchman, and Z. Mróz. FE investigations of the effect of fluctuating local tensile strength on coupled energetic-statistical size effect in concrete beams. *Eng. Struct.*, 103:239–259, 2015.

[34] M. Vořechovský and V. Sadílek. Computational modeling of size effects in concrete specimens under uniaxial tension. *Int. J. Fract.*, 154:27–49, 2008.

[35] Z. J. Yang, X. T. Su, J. F. Chen, and G. H. Liu. Monte Carlo simulation of complex cohesive fracture in random heterogeneous quasi-brittle materials. *Int. J. Solids Struct.*, 46(17):3222–3234, 2009.

[36] F. Zhou and J. F. Molinari. Stochastic fracture of ceramics under dynamic tensile loading. *Int. J. Solids Struct.*, 41:6573–6596, 2004.

List of Figures

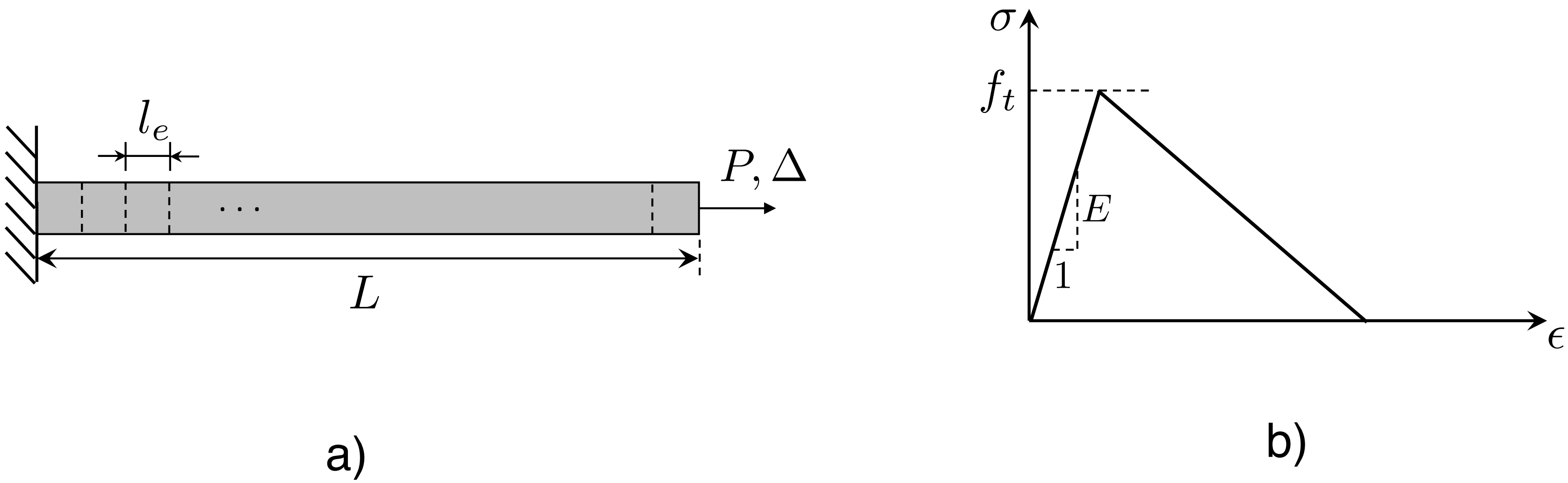

Fig. 1

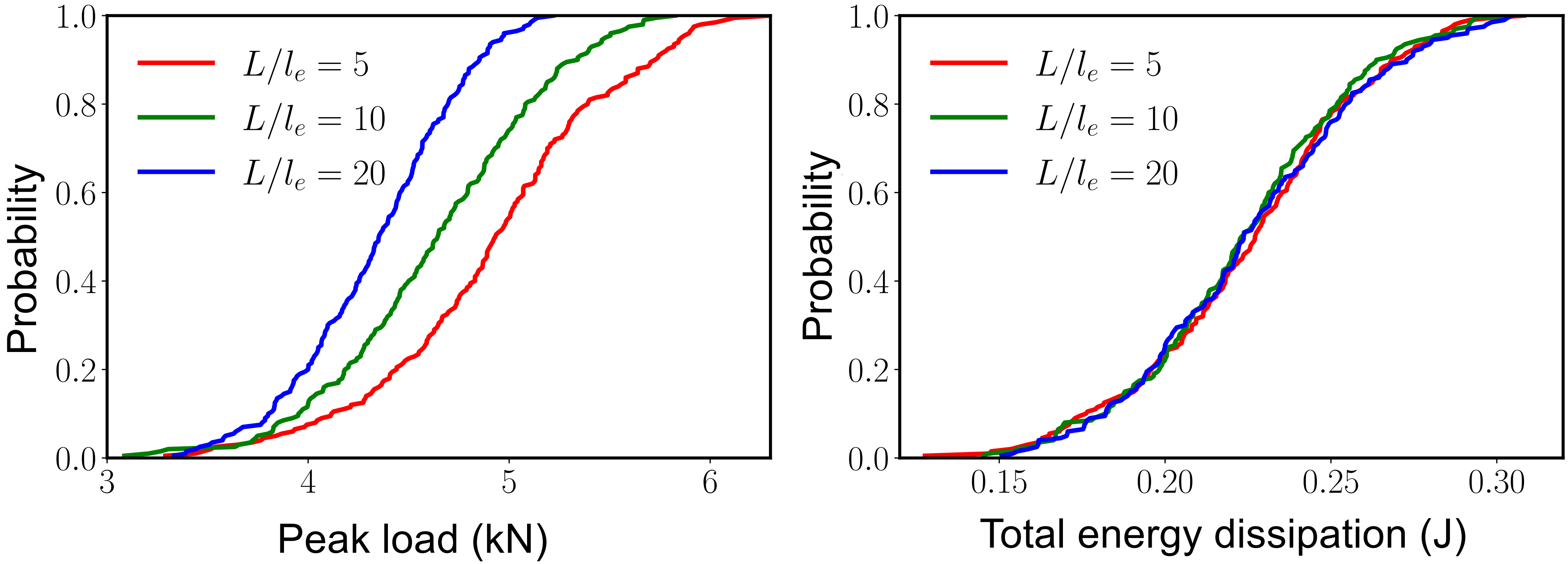

Probability
Peak load (kN)
$L/l_e = 5$
$L/l_e = 10$
$L/l_e = 20$
Total energy dissipation (J)

a) b)

Fig. 2

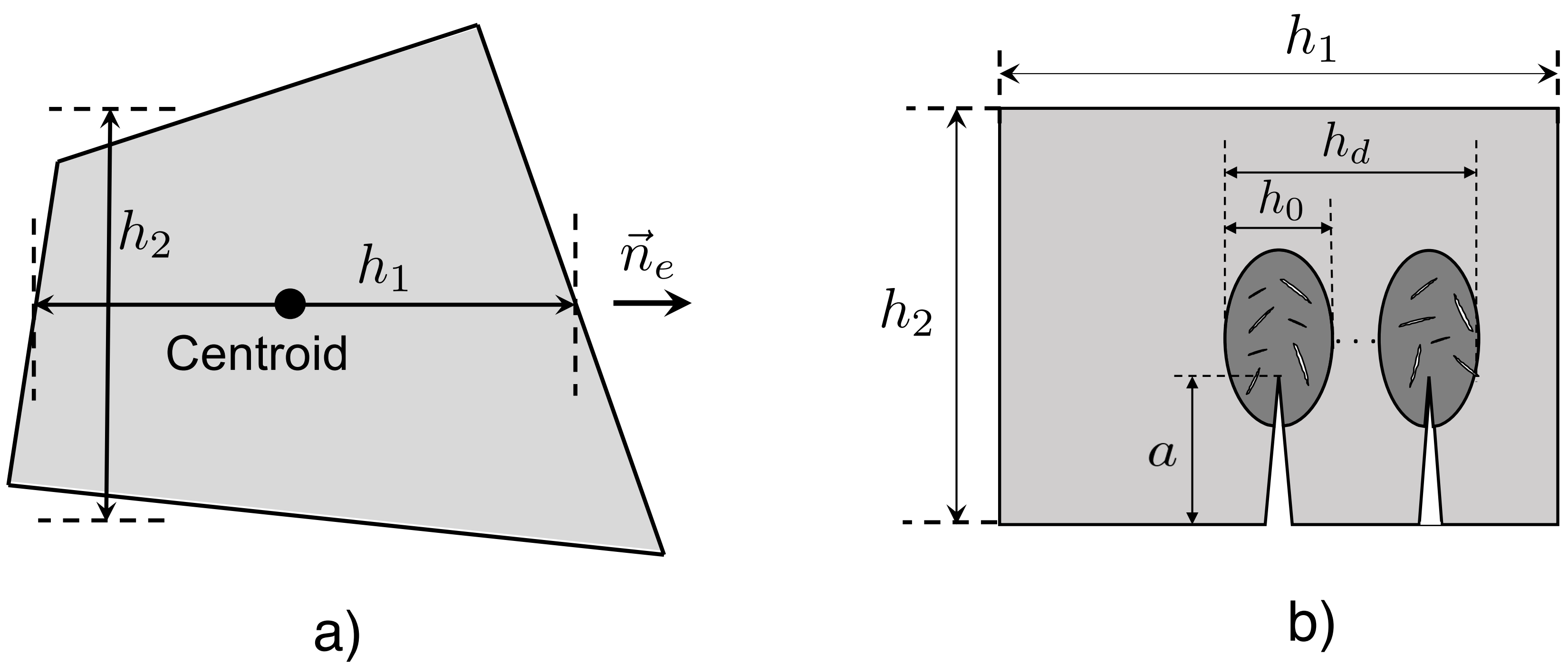

Fig. 3

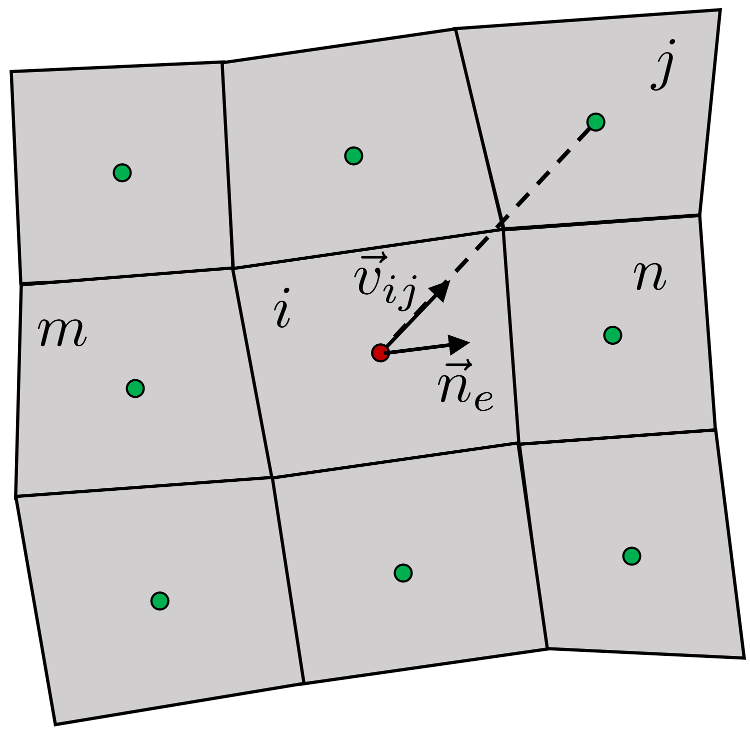

Fig. 4

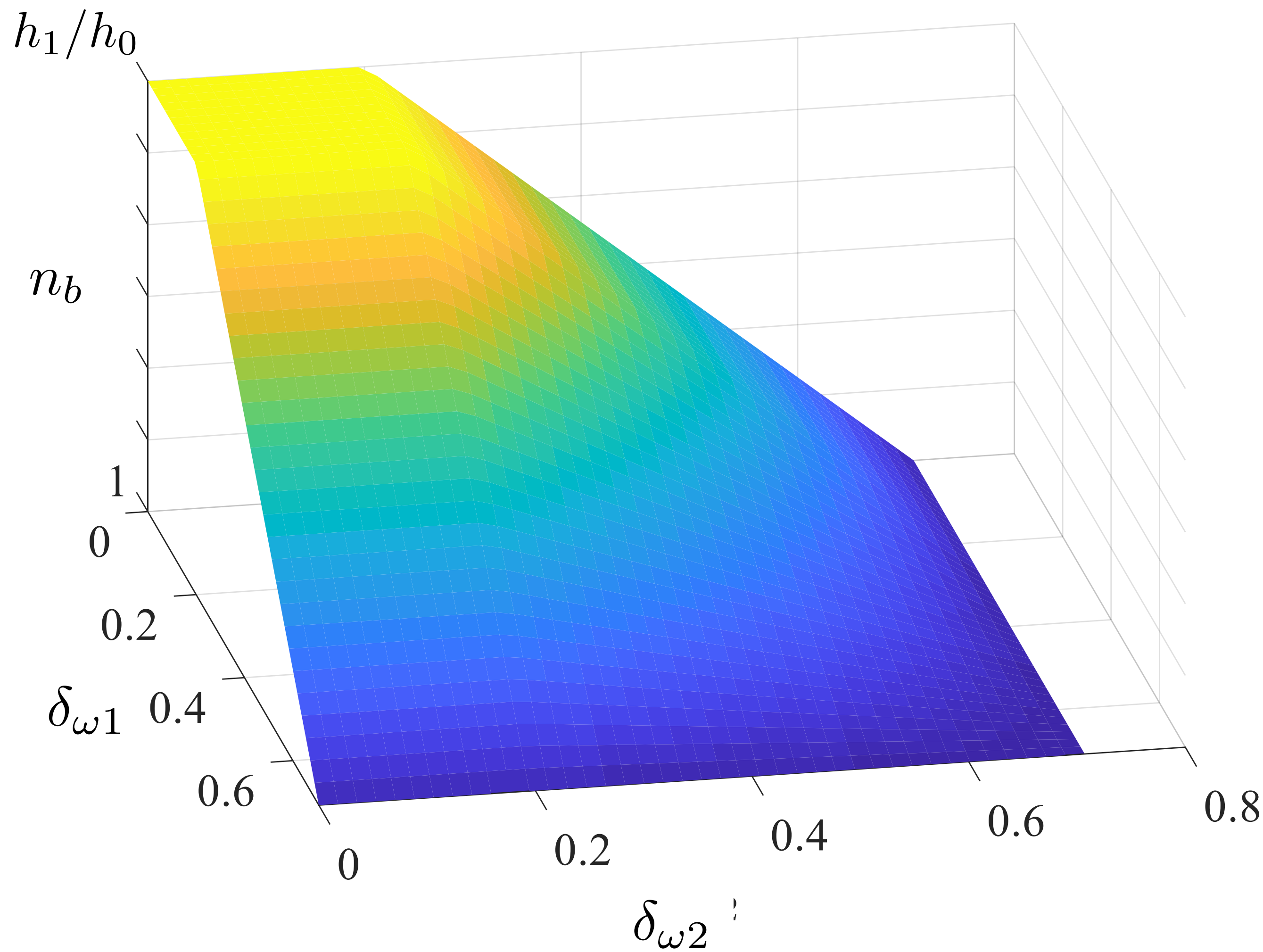

Fig. 5

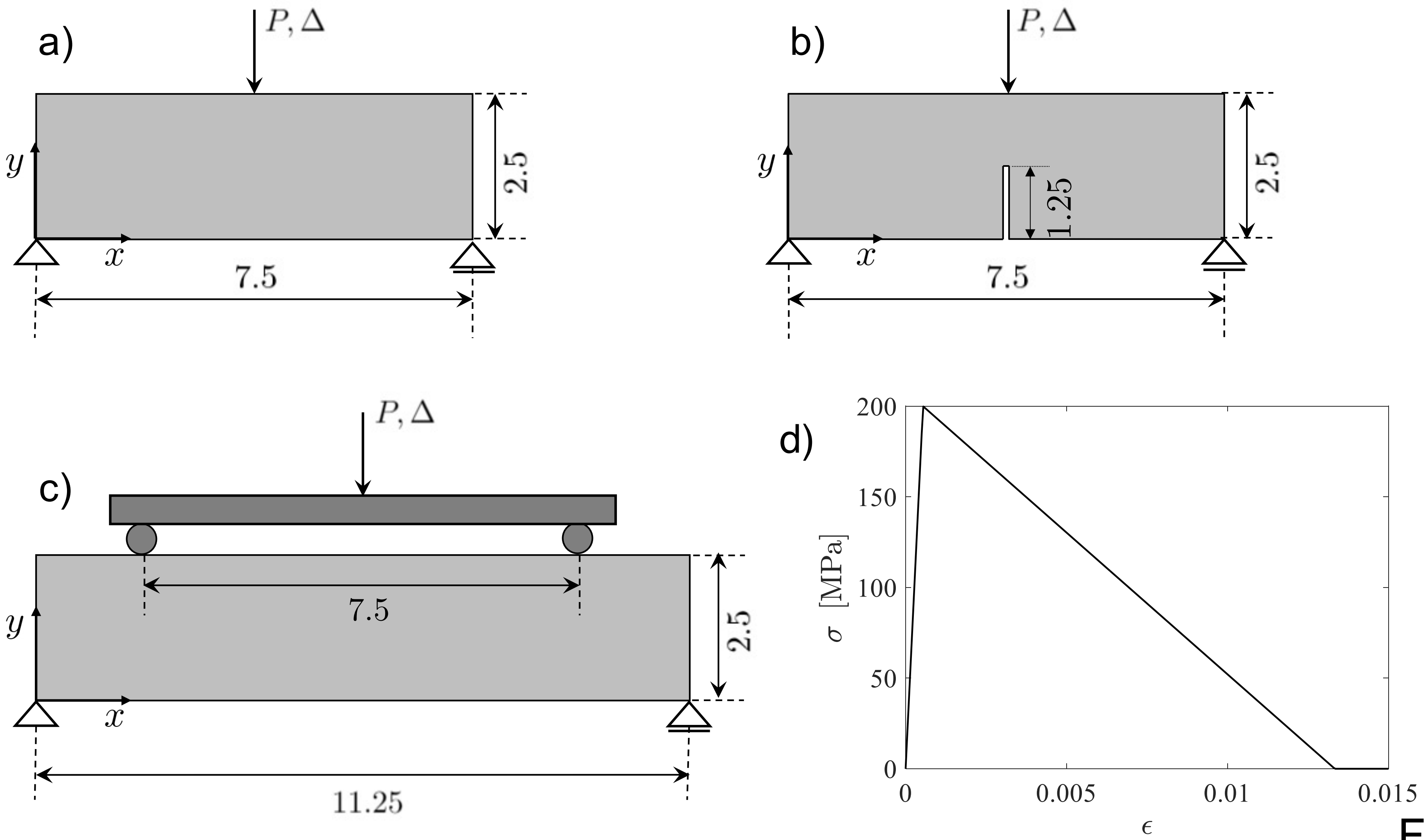
a)
b)
c)
d)
P, Δ
2.5
1.25
7.5
11.25
x
y
σ [MPa]
ϵ
200
150
100
50
0
0.005
0.01
0.015

Fig. 6

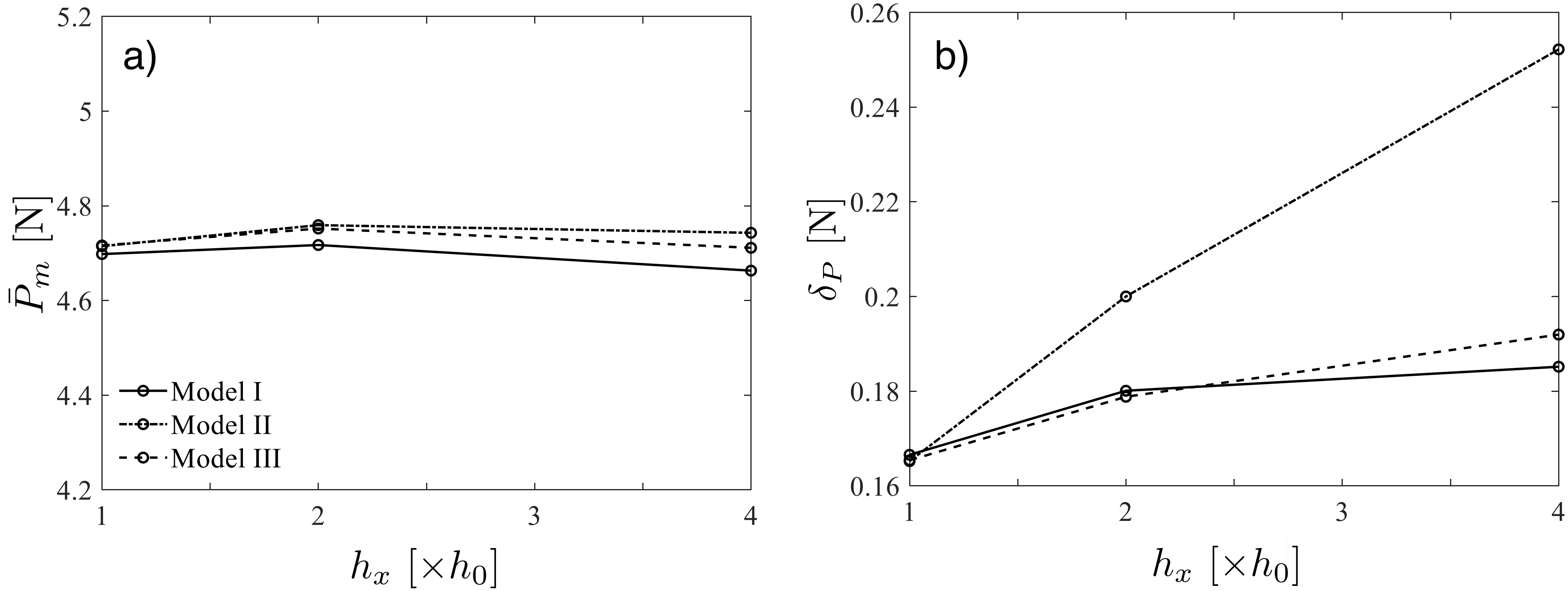

a)
b)
5.2
5
4.8
4.6
4.4
4.2
0.26
0.24
0.22
0.2
0.18
0.16
1
2
3
4
$\bar{P}_m$ [N]
δ_P [N]
h_x [$\times h_0$]
Model I
Model II
Model III

Fig. 7

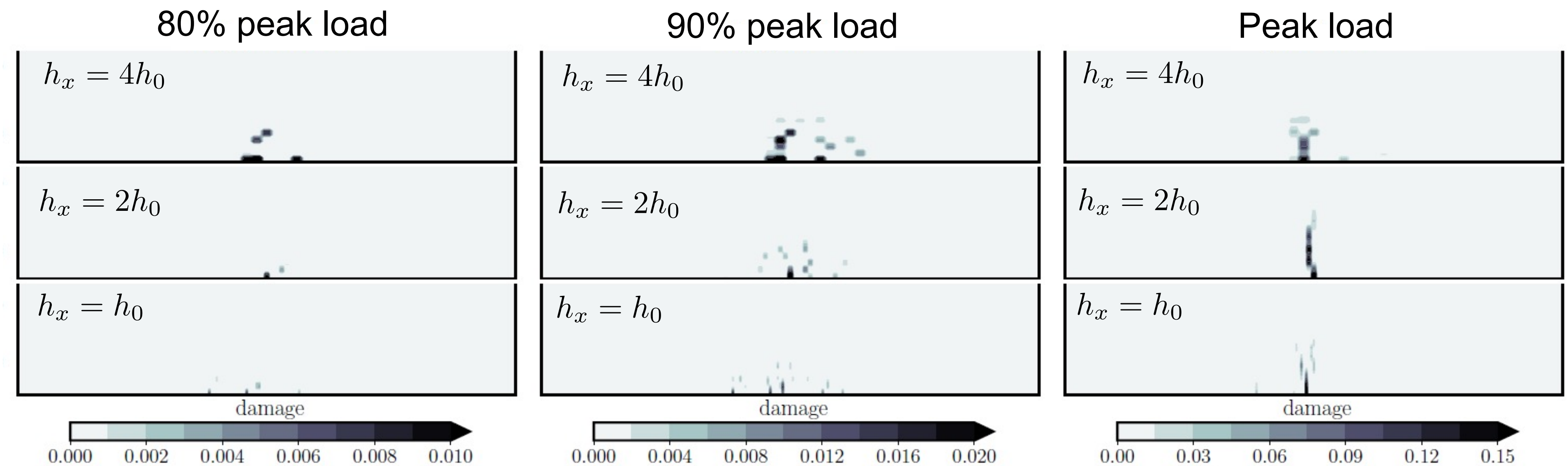
80% peak load
90% peak load
Peak load
$h_x = 4h_0$
$h_x = 2h_0$
$h_x = h_0$
damage
0.000 0.002 0.004 0.006 0.008 0.010
0.000 0.004 0.008 0.012 0.016 0.020
0.00 0.03 0.06 0.09 0.12 0.15

Fig. 8

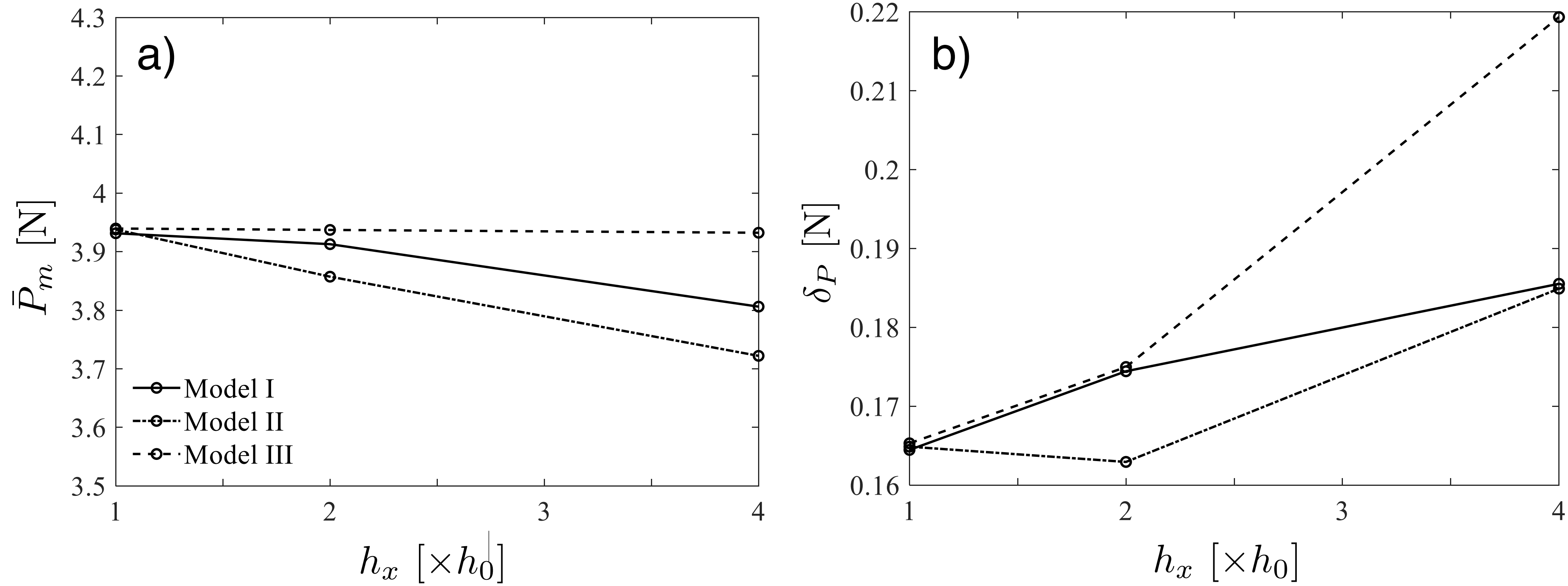
a)
4.3
4.2
4.1
4
3.9
3.8
3.7
3.6
3.5
$\bar{P}_m$ [N]
1
2
3
4
h_x [$\times h_0$]
Model I
Model II
Model III
b)
0.22
0.21
0.2
0.19
0.18
0.17
0.16
δ_P [N]
1
2
3
4
h_x [$\times h_0$]

Fig. 9

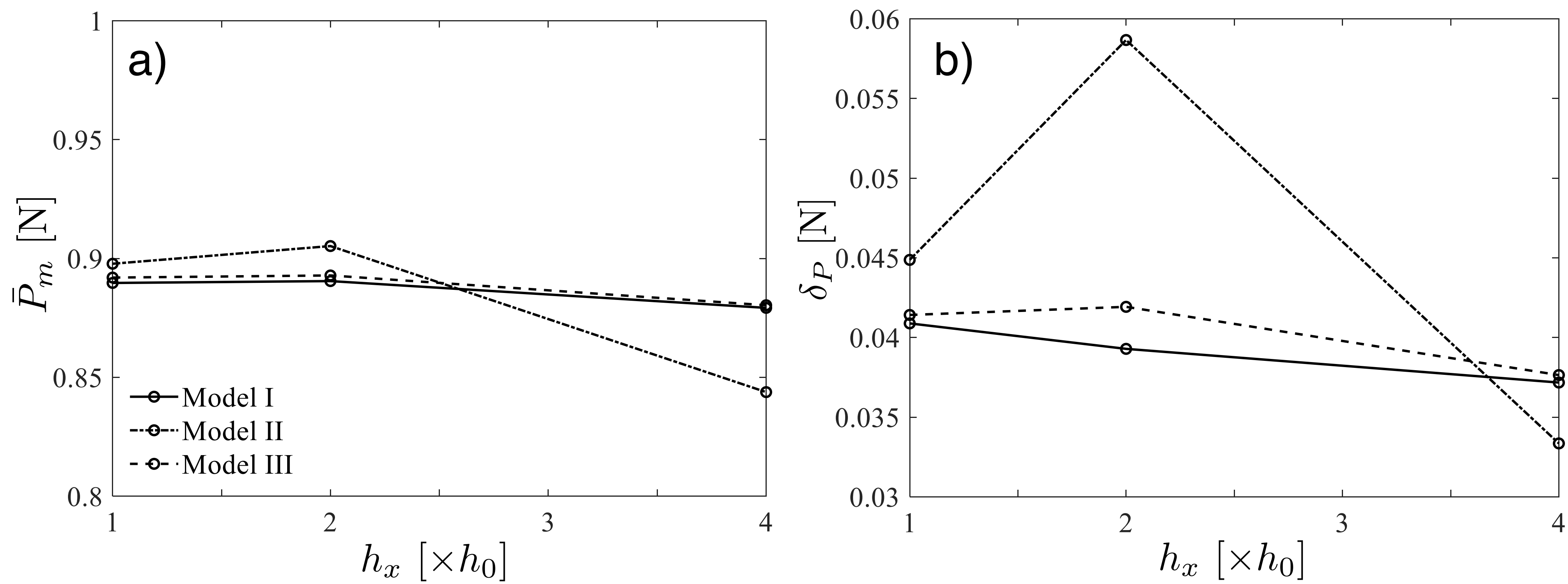

Fig. 10

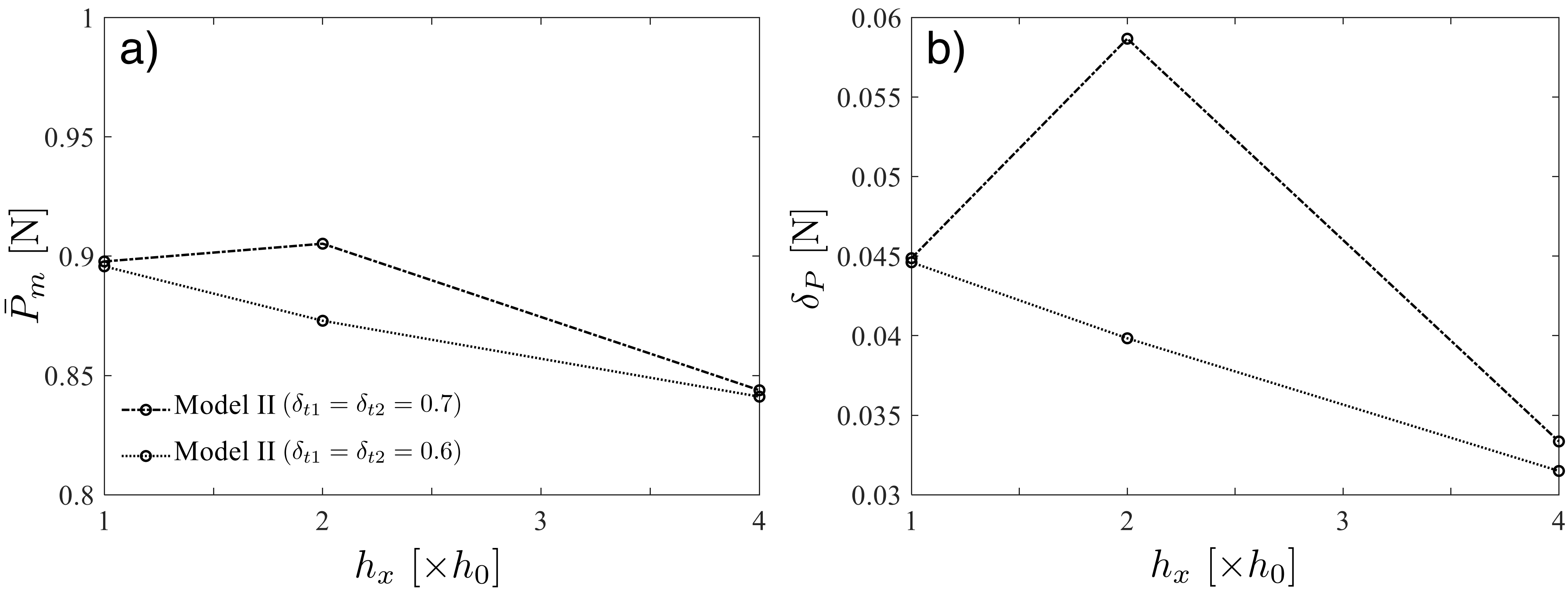

a)
b)
$\bar{P}_m$ [N]
δ_P [N]
h_x [$\times h_0$]
Model II ($\delta_{t1} = \delta_{t2} = 0.7$)
Model II ($\delta_{t1} = \delta_{t2} = 0.6$)

Fig. 11

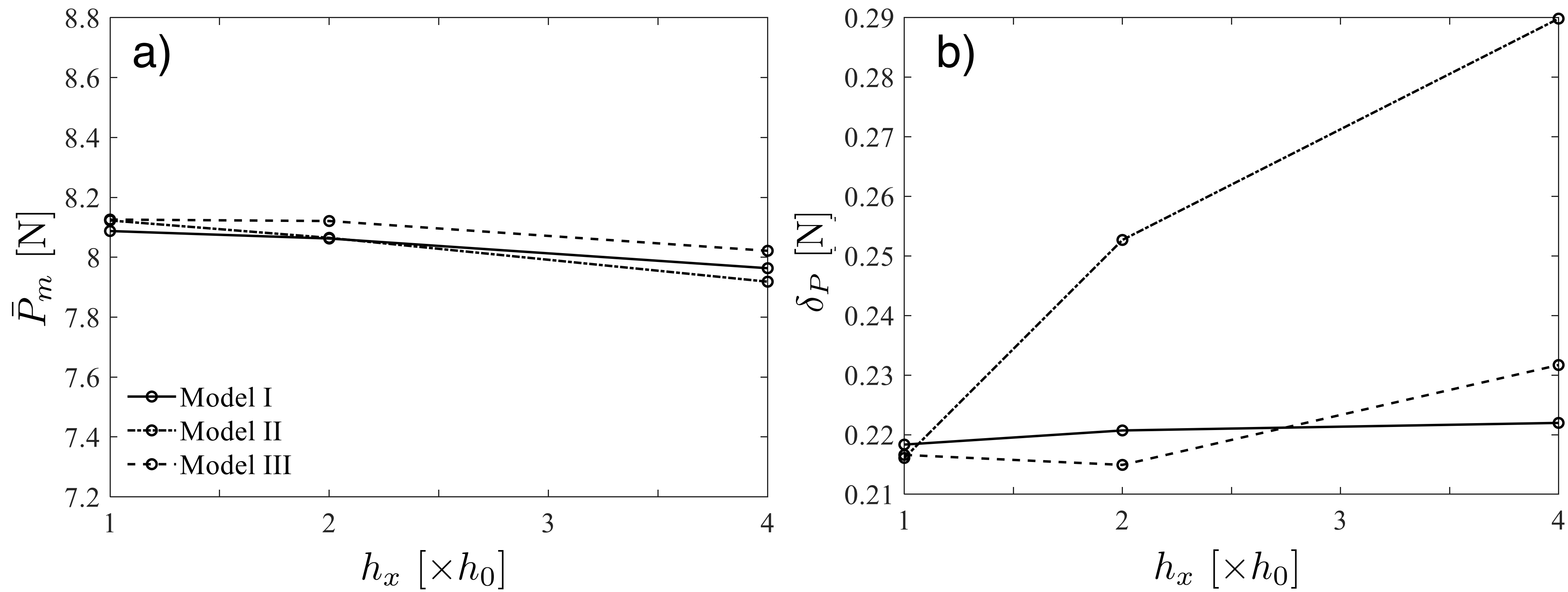
a)
8.8
8.6
8.4
8.2
8
7.8
7.6
7.4
7.2
$\bar{P}_m$ [N]
Model I
Model II
Model III
1
2
3
4
h_x [$\times h_0$]
b)
0.29
0.28
0.27
0.26
0.25
0.24
0.23
0.22
0.21
δ_P [N]
1
2
3
4
h_x [$\times h_0$]

Fig. 12

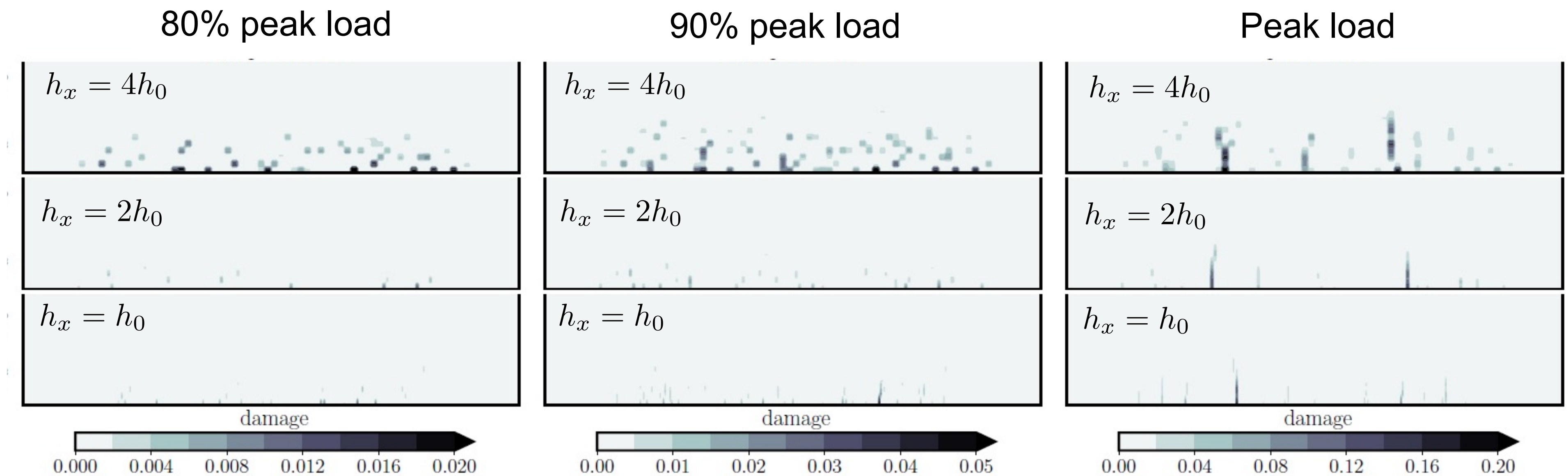
80% peak load
90% peak load
Peak load
$h_x = 4h_0$
$h_x = 2h_0$
$h_x = h_0$
damage
0.000 0.004 0.008 0.012 0.016 0.020
0.00 0.01 0.02 0.03 0.04 0.05
0.00 0.04 0.08 0.12 0.16 0.20

Fig. 13